Eur. Phys. J. D **30**, 123–135 (2004)
DOI: 10.1140/epjd/e2004-00070-x

THE EUROPEAN PHYSICAL JOURNAL D

Quantum fluctuations in holographic teleportation of optical images

A. Gatti[1,a], I.V. Sokolov[2], M.I. Kolobov[3], and L.A. Lugiato[1]

[1] INFM, Dipartimento di Scienze CC FF MM, Università dell'Insubria, via Valeggio 11, 22100 Como, Italy
[2] Physics Institute, St.-Petersburg University, 198904 Petrodvorets, St.-Petersburg, Russia
[3] Laboratoire PhLAM, Université de Lille-1, 59655 Villeneuve d'Ascq Cedex, France

Received 27 October 2003 / Received in final form 16 March 2004
Published online 11 May 2004

Abstract. We investigate in detail the quantum fluctuations in the quantum holographic teleportation protocol that we recently proposed [11]. This protocol implements a continuous variable teleportation scheme that enables the transfer of the quantum state of spatially multimode electromagnetic fields, preserving their quantum correlations in space-time, and can be used to perform teleportation of 2D optical images. We derive a characteristic functional, which provides any arbitrary spatio-temporal correlation function of the teleported field, and calculate the fidelity of the teleportation scheme for multimode Gaussian input states. We show that for multimode light fields one has to distinguish between a global and a reduced fidelity. While the global fidelity tends to vanish for teleportation of fields with many degrees of freedom, the reduced fidelity can be made close to unity by choosing properly the number of essential degrees of freedom and the spatial bandwidth of the EPR beams used in the teleportation scheme.

PACS. 03.67.-a Quantum information – 03.65.Bz Foundations, theory of measurement, miscellaneous theories (including Aharonov-Bohm effect, Bell inequalities, Berry's phase) – 42.50.Dv Nonclassical states of the electromagnetic field, including entangled photon states; quantum state engineering and measurements

1 Introduction

It is well-known that, by following the principles of quantum physics, it is possible to transport an arbitrary quantum state of the electromagnetic field from one place to another using a classical information exchange in combination with a quantum channel which exploits quantum entangled states. This operation, named quantum teleportation, was initially proposed for discrete variables [1] and later extended to continuous-variable schemes [2,3]. Experimental demonstrations for discrete variables were achieved in [4] for single-photon polarization states, and in [5] for continuous variables. In a recent experiment [6] the continuous-variable teleportation scheme of [5] was further improved. Apart from its intrinsic fundamental relevance, the interest towards quantum teleportation also arises from its potential applications in the fields of quantum error correction [7], quantum dense coding [8] and quantum cryptography [9].

The theoretical literature on teleportation considers the case of single-mode fields or, at most, broadband teleportation of time-dependent signals [10]. However, the spatial degrees of freedom offer the opportunity of increasing the number of channels in which teleportation can be realized in parallel. Recently [11] we proposed a protocol to teleport a spatially multimode state of the field. Such a teleportation scheme has a far greater potential as compared to a single-mode case because it enables the simultaneous teleportation of two-dimensional optical images or other two-dimensional data sets. This generalized teleportation scheme opens new potential applications of teleportation for two-dimensional parallel quantum computing, parallel dense coding, error correction.

While at first sight our teleportation scheme seems to be very similar to its single-mode counterpart, the detailed analysis shows that it has several original features which are not present in the single-mode scheme. The most striking difference between the two schemes is the possibility of controlling the performances of the holographic teleportation by optical elements properly inserted into the light beam paths. This possibility of optical control is related to the phenomenon of diffraction which is absent for the single-mode light fields. As it was already outlined in [11], another peculiar feature of the multimode teleportation schemes is the need of using a coarse-grained description of the input and output signals in order to characterize the quality of the teleportation.

In this paper we investigate in detail the quantum noise statistics of the output field in the holographic teleportation protocol proposed in [11], and formulate criteria for achieving a high fidelity of the quantum state

[a] e-mail: alessandra.gatti@mi.infn.it

teleportation. The statistics of the excess noise introduced by the teleportation scheme was described in [11]. The quality of the protocol was there assessed by formulating criteria which ensured that the excess noise was as small as possible. However, no quantitative evaluation of the fidelity of the quantum state transfer was given there. In this paper, we explicitly derive the statistics of the excess noise from a characteristic functional, both in a continuous and in a coarse-grained description of the space-time features of the light fields. The introduction of the characteristic function of the excess noise allows us to calculate the Wigner function of the teleported field from the Wigner function of the input field. In the case of multimode Gaussian states in the input, we are then able to derive an explicit formula for the fidelity of the multimode teleportation process. It turns out that the fidelity not only depends on the features of the quantum noise in each mode of the input state, and on the degree of EPR correlation in the quantum channel (which would be true also in the case of single-mode teleportation), but it also depends on the number and choice of image elements or *pixels* that one wants to teleport in parallel. We will show that, for a large number of degrees of freedom in the input signal, the fidelity of teleportation of the quantum state of the global system tends to be very close to zero. One has to define, therefore, a reduced fidelity of teleportation related to the essential degrees of freedom to be teleported. Such a reduced fidelity can be made close to unity by a proper choice of the spatial bandwidth of the EPR beams used in the protocol as well as by optimization of the scheme with optical devices (lenses) properly inserted in the light beams.

Our investigation allows us to conclude that, in general, the multipixel observables are more sensitive to the lack of entanglement in the quantum channel than the observables for a single pixel.

The paper is organized as follows: in Section 2 we review in more detail the optical scheme of holographic teleportation introduced in [11]. We explain how to create the multimode EPR beams which are an essential part of the teleportation protocol and we provide a physical interpretation of the local spatio-temporal entanglement created by such beams. Section 3 investigates the quantum noise and the spatio-temporal correlation of the teleported optical field. In particular, we derive the characteristic functional describing the statistic of the excess noise introduced by the teleportation protocol, which allows us to evaluate an arbitrary spatio-temporal correlation function at the output of the scheme. This derivation is performed both in a continuous (Sect. 3.1) and in a coarse-grained (Sect. 3.2) description of the field variables. The second kind of description will turn out to be necessary for quantitative characterization of the teleportation fidelity. In Section 4 we derive the Wigner function of the output state, and we calculate the fidelity of the teleportation protocol in the case of Gaussian field statistics in the input. We introduce the concepts of the global and reduced fidelity, and of fidelity per mode, which must be used in order to characterize the quality of holographic teleportation. We make our conclusions in Section 5.

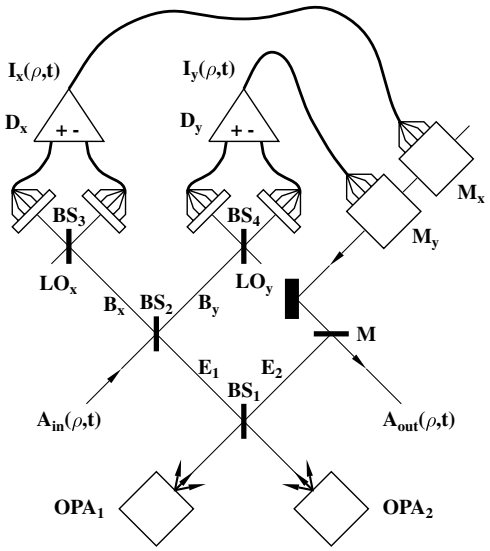

Fig. 1. Scheme of holographic teleportation.

2 Optical scheme for quantum holographic teleportation

The scheme is similar to that proposed and realized in [3,5] and it is shown in Figure 1. The input light field to be teleported from Alice to Bob is described by the field operator $A_{\rm in}(\vec{\rho},t)$, where $\vec{\rho}$ is the 2D transverse coordinate in a cross-section of the beam.

Two quadrature components of the light field are detected "point-by-point" by two homodyne detectors D_x and D_y formed by high-efficiency multipixel photodetection matrices (CCD). The spatio-temporal quantum fluctuations of these quadrature components are locally imprinted into the photocurrents $I_x(\vec{\rho},t)$ and $I_y(\vec{\rho},t)$ at the output of each pixel of the CCD cameras. These photocurrents are sent from Alice to Bob via two multichannel parallel classical communication lines. Bob uses these photocurrents for reconstruction of the field $A_{\rm out}(\vec{\rho},t)$ via two multichannel modulators M_x and M_y which modulate in space and time the relevant quadrature components of an incoming plane coherent light wave. The essential part of the teleportation scheme is a pair of broadband entangled Einstein-Podolsky-Rosen (EPR) light beams. Due to the multimode nature of entanglement our scheme enables the parallel teleportation of N elements of the input wavefront, preserving their space-time correlations. We demonstrated in [11] that this number is given by the ratio of the beam cross-section to the coherence area of the light created by the OPA(s). In the previous teleportation schemes [3,5] $N = 1$.

In our teleportation protocol the multimode EPR beams $E_n(\vec{\rho},t)$, $n = 1,2$, are generated by interference mixing at a 50:50 beam splitter BS_1 of two broadband multimode squeezed beams $S_m(\vec{\rho},t)$, created by

two degenerate traveling-wave OPAs [12–14], as shown in Figure 1. This scheme of generation of the spatially-multimode EPR entanglement is a generalization of the scheme, previously used [5] for the generation of entanglement, which is broadband in time, but single-mode in space. Alternatively, the two multimode EPR beams can be generated by a single traveling-wave OPA, degenerate in frequency, with type-II phase matching [15,16]; in the latter case the two beams have orthogonal polarizations. Below we describe the properties of the broadband multimode squeezing that determine the degree and the spatio-temporal scales of the resulting entanglement.

Homodyne detection of light produced by travelling wave OPA's can be not straightforward to perform, due to the difficulty of matching the temporal and spatial phase profile of the down-converted beam with a local oscillator [17]. A possible solution is to insert the crystal in a resonant cavity. However, in the typical case, the cavity acts as a spatial filter that selects a single transverse mode. An interesting proposal is that of using a confocal optical parametric oscillator [18,19]. Here, thanks to the high mode degeneracy, a good level of squeezing can be achieved in arbitrary small regions of the beam cross-section, at least in the ideal case of [18]. If the finite length of the down-conversion crystal is taken into account, however, it is readily seen that the size of the regions where good squeezing is achieved is again limited by the crystal coherence area [20].

We shall use the space- and time-dependent photon annihilation and creation operators $S_n(\vec{\rho},t)$ and $S_n^\dagger(\vec{\rho},t)$, $n=1,2$, of the squeezed fields. These operators obey [13] the free-field commutation relations,

$$\begin{aligned}\left[S_n(\vec{\rho},t),S_{n'}^\dagger(\vec{\rho}\,',t')\right]&=\delta_{n,n'}\delta(\vec{\rho}-\vec{\rho}\,')\delta(t-t'),\\ [S_n(\vec{\rho},t),S_{n'}(\vec{\rho}\,',t')]&=0,\end{aligned}\tag{2.1}$$

and are normalized so that $\langle S_n^\dagger(\vec{\rho},t)S_n(\vec{\rho},t)\rangle$ gives the mean value of the irradiance, expressed in photons per cm^2 per second.

The light waves $S_m(\vec{\rho},t)$ in the broadband multimode squeezed state are created by two traveling-wave optical parametric amplifiers OPA_1 and OPA_2. The transformation of the input fields $A_m(\vec{\rho},t)$ of the OPAs in the vacuum state into the output fields $S_m(\vec{\rho},t)$ in the broadband multimode squeezed state is described in terms of the Fourier components of these operators in frequency and spatial-frequency domain,

$$s_m(\vec{q},\Omega)=\int d\vec{\rho}\,dt\exp[i(\Omega t-\vec{q}\cdot\vec{\rho})]S_m(\vec{\rho},t).\tag{2.2}$$

In what follows we shall use similar notation for $a_m(\vec{q},\Omega)$ and other field operators. The squeezing transformation performed by the OPAs, can be written as follows:

$$s_m(\vec{q},\Omega)=U_m(\vec{q},\Omega)a_m(\vec{q},\Omega)+V_m(\vec{q},\Omega)a_m^\dagger(-\vec{q},-\Omega),\tag{2.3}$$

where the coefficients $U_m(\vec{q},\Omega)$ and $V_m(\vec{q},\Omega)$ depend on the pump-field amplitudes of the OPAs, their nonlinear susceptibilities and the phase-matching conditions. Here the conditions

$$\begin{aligned}&|U_m(\vec{q},\Omega)|^2-|V_m(\vec{q},\Omega)|^2=1,\\ &U_m(\vec{q},\Omega)V_m(-\vec{q},-\Omega)=U_m(-\vec{q},-\Omega)V_m(\vec{q},\Omega),\end{aligned}\tag{2.4}$$

are necessary and sufficient for preservation of the free-field commutation relations (2.1). The spatial and temporal scales of the squeezed and entangled light fields essentially depend on the orientation angle $\psi_m(\vec{q},\Omega)$ of the major axes of the squeezing ellipses,

$$\psi_m(\vec{q},\Omega)=\frac{1}{2}\arg\left\{U_m(\vec{q},\Omega)V_m(-\vec{q},-\Omega)\right\},\tag{2.5}$$

and on the degree of squeezing $r_m(\vec{q},\Omega)$,

$$e^{\pm r_m(\vec{q},\Omega)}=|U_m(\vec{q},\Omega)|\pm|V_m(\vec{q},\Omega)|.\tag{2.6}$$

The phase of the amplified quadrature components of the OPAs input fields is given [21] by

$$\phi_m(\vec{q},\Omega)=-\frac{1}{2}\arg\left\{U_m(\vec{q},\Omega)V_m^*(-\vec{q},-\Omega)\right\}.\tag{2.7}$$

In analogy to the single-mode EPR beams, the multimode EPR beams are created if squeezing in both channels is effective, and the squeezing ellipses are oriented in the orthogonal directions. For simplicity, we assume that OPA_1 and OPA_2 have such properties that

$$\begin{aligned}U_1(\vec{q},\Omega)&=U_2(\vec{q},\Omega)\equiv U(\vec{q},\Omega),\\ V_1(\vec{q},\Omega)&=-V_2(\vec{q},\Omega)\equiv V(\vec{q},\Omega).\end{aligned}\tag{2.8}$$

These assumptions provide

$$r_1(\vec{q},\Omega)=r_2(\vec{q},\Omega)\equiv r(\vec{q},\Omega),\tag{2.9}$$

$$\psi_1(\vec{q},\Omega)=\psi_2(\vec{q},\Omega)\pm\pi/2\equiv\psi(\vec{q},\Omega),\tag{2.10}$$

$$\phi_1(\vec{q},\Omega)=\phi_2(\vec{q},\Omega)\pm\pi/2\equiv\phi(\vec{q},\Omega).$$

For type-I traveling-wave OPAs, the coefficients $U(\vec{q},\Omega)$ and $V(\vec{q},\Omega)$ are given by [12,22]

$$\begin{aligned}U(\vec{q},\Omega)=\exp\left\{i\left[(k_z(\vec{q},\Omega)-k)l-\delta(\vec{q},\Omega)/2\right]\right\}\\ \times\left[\cosh\Gamma(\vec{q},\Omega)+\frac{i\delta(\vec{q},\Omega)}{2\Gamma(\vec{q},\Omega)}\sinh\Gamma(\vec{q},\Omega)\right],\end{aligned}$$

$$\begin{aligned}V(\vec{q},\Omega)=\exp\left\{i\left[(k_z(\vec{q},\Omega)-k)l-\delta(\vec{q},\Omega)/2\right]\right\}\\ \times\frac{g}{\Gamma(\vec{q},\Omega)}\sinh\Gamma(\vec{q},\Omega).\end{aligned}\tag{2.11}$$

Here l is the length of the nonlinear crystal, $k_z(\vec{q},\Omega)$ is the longitudinal component of the wave vector $\vec{k}(\vec{q},\Omega)$ for the wave with frequency $\omega+\Omega$ and transverse component $\vec{q}$. The dimensionless mismatch function $\delta(\vec{q},\Omega)$ is given by

$$\begin{aligned}\delta(\vec{q},\Omega)&=\Big(k_z(\vec{q},\Omega)+k_z(-\vec{q},-\Omega)-k_p\Big)l\\ &\approx(2k-k_p)l+k''_\Omega l\Omega^2-q^2l/k,\end{aligned}\tag{2.12}$$

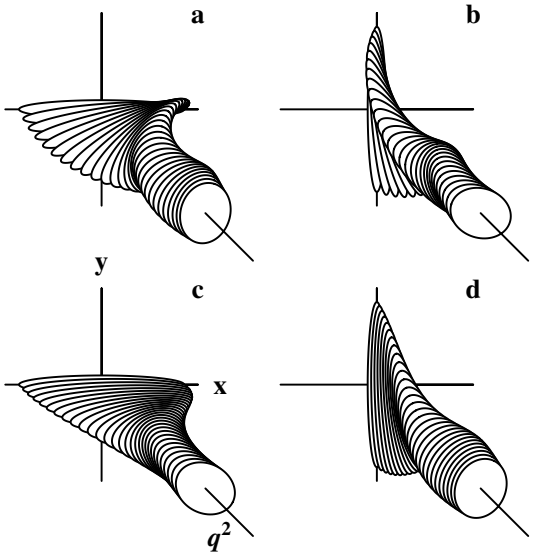

Fig. 2. The squeezing ellipses for the broadband in space-time fields $S_1(\vec{\rho},t)$ (a) and $S_2(\vec{\rho},t)$ (b) in dependence on the mismatch $\delta(\vec{q},\Omega)$ (arbitrary units). The type-I collinear degenerate phase matching, $\exp[r(0,0)]=3$. Figures (c) and (d) show the same squeezing ellipses for the imaging system with a properly inserted lens.

where k_p is the wave number of the pump wave, $k_p-2k=0$ in the degenerate case. We have assumed here the paraxial approximation. The parameter $\Gamma(\vec{q},\Omega)$ is defined as

$$\Gamma(\vec{q},\Omega)=\sqrt{g^2-\delta^2(\vec{q},\Omega)/4}, \tag{2.13}$$

where g is the dimensionless coupling strength of nonlinear interaction, taken real for simplicity. It is proportional to the nonlinear susceptibility, the length of the crystal, and the amplitude of the pump field.

By assuming frequency degenerate and collinear phase-matching condition, when $r(0,0)=g$, one can evaluate the temporal and spatial frequency bandwidths Ω_s and q_s of effective squeezing (see estimates in Sect. IV.D of [13]):

$$\Omega_s=4\sqrt{\frac{1}{|k''_\Omega|l}\frac{g}{\exp[r(0,0)]}},\quad q_s=4\sqrt{\frac{k}{l}\frac{g}{\exp[r(0,0)]}}. \tag{2.14}$$

The spatio-temporal scales of squeezing and entanglement are sensitive to the rotation of the squeezing ellipses in the (x,y)-plane of complex field amplitude with frequencies $\vec{q},\Omega$, i.e. to the frequency dispersion of squeezing. As a result of the rotation, the noise suppression in the given field quadrature goes over to the noise amplification at higher frequencies, as shown in Figures 2a and 2b. This rotation in dependence of the spatial frequency can be effectively eliminated by a properly inserted lens imaging system, see Figures 2c and 2d. The optical control of the spatial scales of squeezing and entanglement will be discussed in more detail in Section 3.

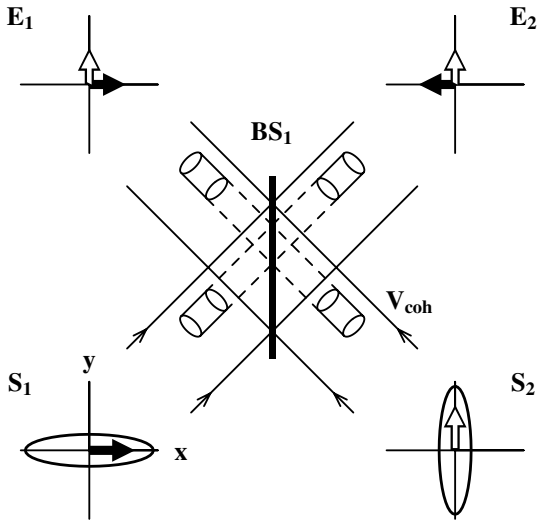

Fig. 3. Generation of the EPR fields $E_1(\vec{\rho},t)$ and $E_2(\vec{\rho},t)$, locally entangled in space-time, via interference of the illuminating squeezed fields $S_1(\vec{\rho},t)$ and $S_2(\vec{\rho},t)$.

The EPR beams $E_n(\vec{\rho},t)$, $n=1,2$, can be created by the interference mixing at the 50:50 beam splitter:

$$E_n(\vec{\rho},t)=\sum_{m=1,2}R_{nm}S_m(\vec{\rho},t). \tag{2.15}$$

Here

$$\{R_{nm}\}=\frac{1}{\sqrt{2}}\begin{pmatrix}1&1\\-1&1\end{pmatrix}, \tag{2.16}$$

is the scattering matrix of the beam splitter. The physical properties of the generated entanglement are illustrated in Figure 3. Consider the corresponding coherence volumes $V_c=cT_cS_c$ in two incident squeezed beams. Here $T_c=2\pi/\Omega_c$ and $S_c=(2\pi/q_c)^2$ are respectively the coherence time and the coherence area, related to the temporal and spatial frequency bandwidths Ω_c and q_c of effective noise suppression in the low-noise quadratures. If the frequency and spatial frequency dispersion of squeezing is corrected, one can assume $\Omega_c\propto\Omega_s$, $q_c\propto q_s$. The left and right lower ellipses in Figure 3 and vectors inside represent the effective local values of the broadband field fluctuations in these coherence volumes. The vectors represent only the stretched (amplified) quadrature amplitudes of the fields S_1 and S_2. The squeezed quadrature amplitudes are negligible for $\exp[r(0,0]\gg 1$ and are not shown. After the scattering, the outgoing fields E_1 and E_2 in the corresponding coherence volumes are composed of the same amplified quadrature amplitudes, see left and right upper plots. This means (in the limit of effective squeezing) the effective correlation and entanglement between the scattered fields: the quadrature amplitudes of the fields E_1 and E_2 coincide (up to the sign, introduced by the unitary transform Eq. (2.16)). In the spatio-temporal domain the entanglement between the broadband fields is local, "volume to volume". In frequency domain the EPR fields are entangled for the frequencies Ω and spatial frequencies $\vec{q}$ within the phase matching of the OPA.

3 Quantum statistics of the teleported field

In order to detect two quadrature components of the input field $A_{\rm in}(\vec{\rho},t)$, this field is splitted at the 50:50 beam splitter BS_2. We shall assume that the scattering matrix of this beam splitter is given by equation (2.16). Another input port of the beamsplitter is illuminated by the EPR beam $E_1(\vec{\rho},t)$. In absence of the EPR beam, which is an essential part of the teleportation scheme, this input port would be illuminated by a broadband in space-time flux of vacuum fluctuations. Thus, the input fields of the balanced homodyne detectors D_x and D_y, used for detection of the x and y field quadratures, read

$$B_{x,y}(\vec{\rho},t)=\frac{1}{\sqrt{2}}\big(\pm A_{\rm in}(\vec{\rho},t)+E_1(\vec{\rho},t)\big), \tag{3.1}$$

with the $+(-)$ sign corresponding to $x(y)$. These fields in turn are mixed with the local oscillator fields LO_x and LO_y having complex amplitudes $B_x^{(H)}=B_0$ and $B_y^{(H)}=iB_0$, where B_0 is real. For parallel teleportation of the local spatio-temporal quantum correlations of the input field, we have first to measure those correlations with spatio-temporal resolution. Temporal resolution can be achieved by choosing properly the frequency bandwidth of a photodetector. In order to resolve spatially the quantum fluctuations we have to use multipixel arrays of photodetectors (like CCD cameras) with pixel size much smaller than the typical spatial scale of quantum correlations. For the case of homodyne detection of spatially single-mode quantum fields, the time-dependent difference photocurrent operators were considered in [23] and, in more general case, in [24]. In the Appendix we shall demonstrate [see Eq. (A.2)] that the difference photocurrent density operators in the balanced homodyne measurement with spatial resolution, performed by D_x and D_y, are expressed through the field operators at the surface of the detectors in analogy to the observables for detection without spatial resolution, formerly investigated by [23,24]

$$\begin{aligned} I_x(\vec{\rho},t)&=B_0\big[B_x(\vec{\rho},t)+B_x^{\dagger}(\vec{\rho},t)\big],\\ I_y(\vec{\rho},t)&=B_0\frac{1}{i}\big[B_y(\vec{\rho},t)-B_y^{\dagger}(\vec{\rho},t)\big]. \end{aligned} \tag{3.2}$$

In particular, these equations provide a correct expression for the spatio-temporal shot noise in the balanced homodyne detection scheme.

The photocurrent densities $I_x(\vec{\rho},t)$ and $I_y(\vec{\rho},t)$ are sent from Alice to Bob via two multichannel classical communication lines. These signals are used by Bob for the independent local modulation of two quadrature components of an external coherent wave, both phase-matched with the relevant quadratures of the EPR fields [2,3,5]. In the modulated beam the field component $\propto I_x(\vec{\rho},t)-iI_y(\vec{\rho},t)$ is created. The teleported field $A_{\rm out}(\vec{\rho},t)$ is obtained by interference mixing at the mirror M with high reflectivity of the modulated field with the second EPR beam E_2 (see Fig. 1),

$$A_{\rm out}(\vec{\rho},t)=E_2(\vec{\rho},t)+g_c\big(I_x(\vec{\rho},t)-iI_y(\vec{\rho},t)\big). \tag{3.3}$$

Here g_c is the coupling constant which takes into account the efficiency of modulation and the transmission of the mirror M. Efficient teleportation takes place when $g_cB_0\sqrt{2}=1$. For a perfect balancing of the mirror reflectivity and modulation gain, as described in [3], the teleported field $A_{\rm out}(\vec{\rho},t)$ takes the form:

$$A_{\rm out}(\vec{\rho},t)=A_{\rm in}(\vec{\rho},t)+F(\vec{\rho},t), \tag{3.4}$$

where

$$F(\vec{\rho},t)=E_2(\vec{\rho},t)+E_1^{\dagger}(\vec{\rho},t), \tag{3.5}$$

is the noise field added by the teleportation process. In the ideal case of perfect entanglement of two EPR beams at all frequencies Ω and spatial frequencies $\vec{q}$ the terms $E_2(\vec{\rho},t)$ and $E_1^{\dagger}(\vec{\rho},t)$ are perfectly anticorrelated and their quantum fluctuation cancel each other. This would correspond to the perfect "point-to-point" in space and instantaneous in time teleportation of the quantum state of the input field with an arbitrary distribution in space and time, $A_{\rm out}(\vec{\rho},t)=A_{\rm in}(\vec{\rho},t)$. However such teleportation would require infinitely large energy of EPR beams. Indeed, first one should achieve an infinite squeezing per single coherence volume of an EPR beam, as in the single-mode case. Additionally, since now we have broadband multimode entanglement, one would need an infinite number of elementary coherence volumes in the EPR beams. In practice teleportation will never be point-to-point in space and instantaneous in time but always "on average" within some spatial area and within some finite time interval.

3.1 Continuous description and field statistics

By using equations (2.15) and (2.3), for the noise amplitude given by equation (3.5), we obtain in the Fourier domain

$$f(\vec{q},\Omega)=\xi^*(-\vec{q},-\Omega)c_1^{\dagger}(-\vec{q},-\Omega)+\xi(\vec{q},\Omega)c_2(\vec{q},\Omega), \tag{3.6}$$

where

$$\xi(\vec{q},\Omega)=U(\vec{q},\Omega)-V^*(-\vec{q},-\Omega), \tag{3.7}$$

and the field operators

$$c_{1,2}(\vec{q},\Omega)=\frac{1}{\sqrt{2}}\big(\pm a_1(\vec{q},\Omega)+a_2(\vec{q},\Omega)\big), \tag{3.8}$$

with the $+(-)$ sign corresponding to 1(2), are unitary superpositions of two independent vacuum fields on the inputs of the OPAs. The fields $c_{1,2}(\vec{q},\Omega)$ are also in vacuum state. An immediate consequence of equations (2.4) and (3.6) is that the noise operators have the commutation relations of a classical field:

$$\begin{aligned} \big[f(\vec{q},\Omega),f^{\dagger}(\vec{q}\,',\Omega')\big]&=(2\pi)^3\delta^2(\vec{q}-\vec{q}\,')\delta(\Omega-\Omega')\\ &\quad\times\big(|\xi(\vec{q},\Omega)|^2-|\xi(-\vec{q},-\Omega)|^2\big)=0,\\ [f(\vec{q},\Omega),f(\vec{q}\,',\Omega')]&=0, \end{aligned} \tag{3.9}$$

and thus can be considered as classical noise forces. Actually, as a consequence of (2.11), one has $|V(\vec{q},\Omega)| = |V(-\vec{q},-\Omega)|$, and the function $\xi(\vec{q},\Omega)$ in (3.6) is found in the form

$$\xi(\vec{q},\Omega) = e^{-i\phi(\vec{q},\Omega)}\Big\{e^{-r(\vec{q},\Omega)}\cos\psi(\vec{q},\Omega) + ie^{r(\vec{q},\Omega)}\sin\psi(\vec{q},\Omega)\Big\}. \quad (3.10)$$

In the spatio-temporal domain the noise field $F(\vec{\rho},t)$ is given by

$$F(\vec{\rho},t) = \frac{1}{(2\pi)^3}\int d\vec{\rho}_0 dt_0\Big\{\xi^*(\vec{\rho}-\vec{\rho}_0,t-t_0)C_1^\dagger(\vec{\rho}_0,t_0) + \xi(\vec{\rho}-\vec{\rho}_0,t-t_0)C_2(\vec{\rho}_0,t_0)\Big\}. \quad (3.11)$$

The statistics of this noise field are determined in the most general form by the characteristic functional,

$$\tilde{\chi}(\lambda,\lambda^\star) = \langle in|\exp\Big\{\int d\vec{\rho}\,dt\Big(\lambda(\vec{\rho},t)F^\dagger(\vec{\rho},t) - \lambda^\star(\vec{\rho},t)F(\vec{\rho},t)\Big)\Big\}|in\rangle. \quad (3.12)$$

We calculate the functional (3.12) by normally ordering the field operators $C_n(\vec{\rho},t)$, $C_n^\dagger(\vec{\rho},t)$, where $n = 1,2$, in the exponent with the use of the standard transformation, $\exp(A+B) = \exp B\exp A\exp([A,B]/2)$. Taking into account the free-field commutation relations, analogous to (2.1), and the vacuum boundary condition $C_n(\vec{\rho},t)|in\rangle = 0$, after some calculation we obtain:

$$\tilde{\chi}(\lambda,\lambda^\star) = \exp\Big\{-\int d\vec{\rho}\,d\vec{\rho}'\,dt\,dt'\lambda(\vec{\rho},t)\lambda^\star(\vec{\rho}',t') \times G(\vec{\rho}-\vec{\rho}',t-t')\Big\}, \quad (3.13)$$

where the Fourier transform of the Green function $G(\vec{\rho},t)$ reads

$$G(\vec{q},\Omega) = |\xi(\vec{q},\Omega)|^2 = e^{-2r(\vec{q},\Omega)}\cos^2\psi(\vec{q},\Omega) + e^{2r(\vec{q},\Omega)}\sin^2\psi(\vec{q},\Omega). \quad (3.14)$$

It follows from equation (3.13) that the noise is Gaussian. At any order, the spatio-temporal correlation functions of the fields $F(\vec{\rho},t)$ and $F^\dagger(\vec{\rho},t)$ can be expressed in a standard way via the second-order correlation functions

$$\langle F(\vec{\rho},t)F^\dagger(\vec{\rho}',t')\rangle = G(\vec{\rho}-\vec{\rho}',t-t'), \quad (3.15)$$

$$\langle F(\vec{\rho},t)F(\vec{\rho}',t')\rangle = 0\,. \quad (3.16)$$

More precisely we have

$$\left\langle\prod_{n,\,m=1}^{N}F(\vec{\rho}_n,t_n)F^\dagger(\vec{\rho}_m,t_m)\right\rangle = \lim_{\lambda,\lambda^\star\to 0}\left\{\prod_{n,\,m=1}^{N}\frac{\partial}{\partial\lambda(\vec{\rho}_n,t_n)}\frac{\partial}{\partial\lambda^\star(\vec{\rho}_m,t_m)}\right\}\tilde{\chi}(\lambda,\lambda^\star) = \sum_P\left\{\prod_{n,\,m=1}^{N}\langle F(\vec{\rho}_n,t_n)F^\dagger(\vec{\rho}_{p_n},t_{p_n})\rangle\right\}. \quad (3.17)$$

The sum over P in equation (3.17) means the sum over all possible permutations $(p_1,...,p_N)$ of labels $(1,...,N)$. Correlation functions containing a different number of creation and annihilation noise operators vanish, because of equation (3.16). Notice that in the above the operator ordering is irrelevant because the noise operators commute.

Incidentally, a similar Green function describes the photocurrent correlations in space-time by the homodyne detection of multimode squeezed light [25].

When squeezing and entanglement are not present, $r(\vec{q},\Omega) = 0$, the Green function is δ-correlated in space-time,

$$G(\vec{\rho},t) = \delta(\vec{\rho})\delta(t). \quad (3.18)$$

When entanglement is present over the spatial and temporal scales S_c, T_c and for $\psi(0,0) = 0$, a positive δ-correlated term similar to that in equation (3.18) is accompanied by a negative term due to spatio-temporal anticorrelations on the scales S_c, T_c. This anticorrelation permits the suppression of the averaged noise field, as we shall discuss in detail in the section below.

The spatial scales of the noise suppression are sensitive to the rotation of squeezing ellipses in dependence of the spatial frequency, shown in Figures 2a and 2b. In the spatial-frequency domain this is evident from the behavior of the Green function (3.14), where the amplified quadrature amplitudes of noise are present with the weight $\propto \sin^2\psi(\vec{q},\Omega) \neq \sin^2\psi(0,0) = 0$. The misalignment of squeezing ellipses increases with propagation along the crystal and in free space and leads to the diffraction spread of the coherence area. A properly inserted lens imaging system compensates [12] this misalignment, as shown in Figures 2c and 2d, and brings the size of the coherence area S_c to its optimum value. If the squeezing, generated by the OPAs, is effective for $q \le q_s$, this value is evaluated as $S_c = (2\pi/q_s)^2$.

In order to compensate diffraction, one can insert the lenses directly into the EPR beams E_n, $n = 1,2$. In the general case this effect is described by phase shifts quadratic in q, $\theta_n(q) = \gamma_n q^2$ [13]:

$$E_n(\vec{q},\Omega) \to \tilde{E}_n(\vec{q},\Omega) = E_n(\vec{q},\Omega)e^{i\theta_n(q)}. \quad (3.19)$$

By accounting for this phase correction in equations (3.4) and (3.5) we find the corrected orientation angle $\psi(\vec{q},\Omega) \to \tilde{\psi}(\vec{q},\Omega) = \psi(\vec{q},\Omega) + \theta(q)$, where $\theta(q) = (\theta_1(q)+\theta_2(q))/2$. This angle should be substituted into the Green function (3.14), $G(\vec{q},\Omega) \to \tilde{G}(\vec{q},\Omega)$. The best

result that can be obtained with lenses is to set $\theta(q) = -[\mathrm{d}^2\psi/\mathrm{d}q^2]_{q=0}\, q^2$, as in Figures 2c and 2d. With this choice $\tilde{\psi}(\vec{q},0) \approx 0$ and $\tilde{G}(q,0) \approx e^{-2r(q,0)}$ over a broad range of q. Physically speaking, lenses compensate the effect of diffraction on the spatial scale of entanglement. For two entangled fields the lens arrangement can be asymmetric, since only the net phase shift $\theta(q)$ is of importance.

3.2 Coarse-grained description and field quadrature statistics

As mentioned above, the multimode teleportation will always be "on average" within some finite spatial area and some finite time interval. Therefore, in order to quantitatively characterize the performances of the scheme, we have to introduce a coarse-grained description of the input and output variables. We consider averaging of the field variables over a pixel S_j of area $S = \Delta^2$ and over a time window T_i of duration T:

$$A_{\mathrm{out}}(j,i) = \frac{1}{\sqrt{ST}} \int_{S_j} d\vec{\rho} \int_{T_i} dt\, A_{\mathrm{out}}(\vec{\rho},t), \tag{3.20}$$

with analogous definitions for the input field. The averaged field operators obey standard commutation relations

$$[A_{\mathrm{out}}(j,i), A^{\dagger}_{\mathrm{out}}(j',i')] = \delta_{j,j'}\delta_{i,i'}, \tag{3.21}$$

and hence correspond to a discrete subset of field oscillators.

Next, we consider generic field quadrature operators of the output and input field

$$X^{\varphi}_{\mathrm{out/in}}(j,i) = A_{\mathrm{out/in}}(j,i)e^{-i\varphi} + A^{\dagger}_{\mathrm{out/in}}(j,i)e^{i\varphi}, \tag{3.22}$$

$$Y^{\varphi}_{\mathrm{out/in}}(j,i) = -iA_{\mathrm{out/in}}(j,i)e^{-i\varphi} + iA^{\dagger}_{\mathrm{out/in}}(j,i)e^{i\varphi}. \tag{3.23}$$

These are observables which can be measured by means of homodyne detection with a high efficiency CCD camera. By using equation (3.4) we obtain,

$$X^{\varphi}_{\mathrm{out}}(j,i) = X^{\varphi}_{\mathrm{in}}(j,i) + \mathcal{X}_{\varphi}(j,i), \tag{3.24}$$

$$Y^{\varphi}_{\mathrm{out}}(j,i) = Y^{\varphi}_{\mathrm{in}}(j,i) + \mathcal{Y}_{\varphi}(j,i). \tag{3.25}$$

where the excess noise added by the teleportation process on the measured field quadrature is given by

$$\mathcal{X}_{\varphi}(j,i) = \frac{1}{\sqrt{ST}} \int_{S_j} d\vec{\rho} \int_{T_i} dt \left[F(\vec{\rho},t)e^{-i\varphi} + F^{\dagger}(\vec{\rho},t)e^{i\varphi}\right], \tag{3.26}$$

$$\mathcal{Y}_{\varphi}(j,i) = \frac{1}{\sqrt{ST}} \int_{S_j} d\vec{\rho} \int_{T_i} dt \left\{-i\left[F(\vec{\rho},t)e^{-i\varphi} - F^{\dagger}(\vec{\rho},t)e^{i\varphi}\right]\right\}. \tag{3.27}$$

As follows from equations (3.13–3.15), these operators are a linear combination of Gaussian stochastic variables, independent of the input. Hence the set

$$\{\mathcal{X}_{\varphi}(j,i),\, \mathcal{Y}_{\varphi}(j,i)\}_{j,i}, \tag{3.28}$$

represent a set of classical Gaussian stochastic variables. Here $j = 1,\ldots N$, $i = 1,\ldots K$, is a finite set of indices labeling the pixels and the time intervals of interest. These variables are independent of the input field and have zero mean values. Their statistical properties are completely described in terms of a characteristic function

$$\chi_{\mathrm{noise}}\left(\{\mu_{ji},\nu_{ji}\}\right) = \left\langle \exp\left\{ i \sum_{j,i} \left(\mu_{ji}\mathcal{X}_{\varphi}(j,i) + \nu_{ji}\mathcal{Y}_{\varphi}(j,i)\right)\right\}\right\rangle = \exp\left\{ -\frac{1}{2} \sum_{j,j';i,i'} \mathcal{C}(j,j';i,i')\left(\mu_{ji}\mu_{j'i'} + \nu_{ji}\nu_{j'i'}\right)\right\}, \tag{3.29}$$

where the covariance matrix is defined as

$$\mathcal{C}\,(j,j'\,;\,i,i') = \langle \mathcal{X}_{\varphi}(j,i)\,\mathcal{X}_{\varphi}(j',i')\rangle = \langle \mathcal{Y}_{\varphi}(j,i)\,\mathcal{Y}_{\varphi}(j',i')\rangle. \tag{3.30}$$

The covariance matrix elements are found with the use of equations (3.26), (3.27), (3.15), (3.20), and (3.23). They can be expressed in terms of the Green function in equation (3.13) as

$$\mathcal{C}\,(j,j'\,;\,i,i') = 2\int \mathrm{d}\vec{q}\, B_{\Delta}(\vec{q}) B_T(\Omega) \times \cos\left[\vec{q}\cdot(\vec{\rho}_j - \vec{\rho}_{j'}) - \Omega(t_i - t_{i'})\right]\tilde{G}(\vec{q},\Omega), \tag{3.31}$$

where $\vec{\rho}_j$ is the center of the pixel j, and t_i is the center of the ith time interval. Here $\tilde{G}(\vec{q},\Omega)$ is the Green function (3.14) with the corrected value of the orientation angle $\tilde{\psi}(\vec{q},\Omega) = \psi(\vec{q},\Omega) + \theta(\vec{q})$. In equation (3.31) functions $B_{\Delta}(\vec{q})$ $B_T(\Omega)$ arise from the coarse-graining operation. For e.g. a square pixel of side Δ they read,

$$B_{\Delta}(\vec{q}) = \frac{\Delta^2}{4\pi^2}\mathrm{sinc}^2\left(\frac{q_x\Delta}{2}\right)\mathrm{sinc}^2\left(\frac{q_y\Delta}{2}\right) \overset{\Delta\to\infty}{\to} \delta(\vec{q}), \tag{3.32}$$

$$B_T(\Omega) = \frac{T}{2\pi}\mathrm{sinc}^2\left(\frac{\Omega T}{2}\right) \overset{T\to\infty}{\to} \delta(\Omega). \tag{3.33}$$

Incidentally, we notice that the covariance matrix (3.31) does not depend on the phase φ of the local oscillator, used for the homodyne detection, so that the added noise is the same for any quadrature component.

Ideal teleportation takes place when the Gaussian distribution of noise has a vanishing small width in all directions of phase space, so that it approximates a multivariate Dirac δ-function. This can be realized if both the time window T and the pixel size Δ are large enough, so that the functions (3.32) and (3.33) in the integral of equation (3.31) filter a band of temporal and spatial frequencies well inside the squeezing bandwidths, where $G(\vec{q},\Omega) \ll 1$. When the pixel side Δ and the time window T are much larger than the OPA coherence length l_c, and the OPA coherence time T_c, respectively, we obtain

$$\lim_{\Delta\to\infty\,,T\to\infty} \mathcal{C}\,(j,j'\,;\,i,i') = 2\delta_{j,j'}\delta_{i,i'}\exp(-2r(0,0)). \tag{3.34}$$

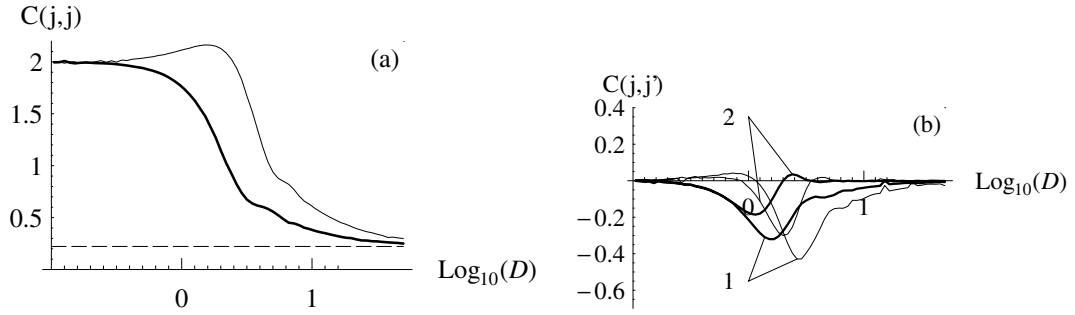

Fig. 4. Covariance matrix elements of the noise added by the teleportation scheme as a function of $D = \Delta/l_d$. The squeezing parameter is $\exp[r(0,0)] = 3$. Figure (a) shows the diagonal element $\mathcal{C}(j,j)$ of the covariance matrix for observation without (thin line) and with (bold line) a correcting lens. Figure (b) shows off-diagonal elements $\mathcal{C}(j,j')$ with $|\vec{\rho}_j - \vec{\rho}_{j'}| = \Delta$ (lines 1), and with $|\vec{\rho}_j - \vec{\rho}_{j'}| = \sqrt{2}\Delta$ (lines 2). Bold and thin lines have the same meaning as on (a).

In addition, as in the single-mode case, a large degree of EPR correlation (large squeezing parameter r), is required in order to achieve a good quality teleportation.

For a broadband OPA, where the parametric crystal length is on the order of millimeters, the coherence time is of the order of femtoseconds to picoseconds, so that usual detection time windows overcome by several order of magnitudes the coherence time. Hence, in equation (3.31) it is reasonable to assume the limit $T \gg T_c$, under which the noise added by the teleportation scheme is uncorrelated in time,

$$\mathcal{C}\,(j,j'\,;i,i') = \langle \mathcal{Y}_\varphi(j,i)\,\mathcal{Y}_\varphi(j',i')\rangle = \delta_{i,i'}\mathcal{C}(j,j'). \quad (3.35)$$

However, the same is not true for the spatial domain. For example, for an OPA with a 3 mm long crystal, at $\lambda = 0.712$ μm, taking as a rough estimate for the coherence length l_c the diffraction spread l_d at the crystal exit, we arrive to

$$l_c \sim l_d = \sqrt{l/2k} = 13\ \mu\text{m}. \quad (3.36)$$

Provided that the spatial extent in the transverse plane where EPR correlations do exist is limited by the pump spot size, choosing $\Delta \gg l_c$ would amount to integrating over the whole beam cross-section and losing all spatial information.

In Figure 4 we illustrate the role of the pixel size for the noise added by the teleportation process. Precisely, we plot our numerical calculations for some elements of the covariance matrix in the limit $T \gg T_c$ as a function of the ratio of the pixel side to the diffraction length $D = \Delta/l_d$, where l_d is defined by equation (3.36). As our system has an overall translational symmetry, the covariance matrix elements $\mathcal{C}(j,j')$ depend only on the relative distance and on the orientation of pixels with respect to the difference position vector $(\vec{\rho}_j - \vec{\rho}_{j'})$. In particular, all the diagonal elements $\mathcal{C}(j,j)$ have the same value.

Figure 4a shows the diagonal element $\mathcal{C}(j,j)$ of the covariance matrix. The wide and narrow solid lines correspond to the observation with (bold lines) and without (thin lines) diffraction phase shift compensation with the use of a lens arrangement. In both cases the plot for the diagonal element $\mathcal{C}(j,j)$ shows the classical limit $\mathcal{C}(j,j) \to 2$ for small pixel size, when the contribution of the high-frequency Fourier components of the noise field, $q \gg q_c$, remaining in the vacuum state, dominates. On the other side, when the pixel size is of the same order of magnitude as the coherence length, both the wide and narrow lines rapidly approach the $\Delta \to \infty$ limit of equation (3.34), $\mathcal{C}_(j,j) \to 2\exp[-2r(0,0)]$ (dashed line), which corresponds to the single-mode quantum teleportation limit. This behavior should be compared with the covariance matrix of the noise in a classical teleportation scheme, i.e. in the absence of the EPR correlations. Then $r(\vec{q},\Omega) = 0$, $\mathcal{C}_{\rm cl}(j,j') = 2\delta_{j,j'}$, and $\mathcal{C}_{\rm cl}(j,j) = 2$. In this limit two units of vacuum noise are added at each pixel, just as in the case of the single-mode teleportation [5]. Figure 4b shows some off-diagonal elements of the covariance matrix as a function of Δ/l_d. They show correlations between the nearest neighbor pixels in a row or a column, $|\vec{\rho}_j - \vec{\rho}_{j'}| = \Delta$ (lines 1), and between the pixels on a diagonal $|\vec{\rho}_j - \vec{\rho}_{j'}| = \sqrt{2}\Delta$ (lines 2), of the detector matrix. As can be seen from these plots, when the pixel side is small compared to the coherence length, our teleportation scheme not only adds noise on each pixel (as in the single-mode scheme) but also introduces correlations between pixels. The existence of spatial correlations over distances on the order of the coherence length is typical of the multimode squeezed light, and has been investigated in detail e.g. in [25,26].

4 Fidelity of the holographic teleportation

Using equation (3.24) we can obtain the explicit relation between the spatio-temporal correlation functions of the field quadratures in the output and in the input,

$$\langle \delta X^{\varphi}_{\rm out}(j,i)\,\delta X^{\varphi}_{\rm out}(j',i')\rangle = \langle \delta X^{\varphi}_{\rm in}(j,i)\,\delta X^{\varphi}_{\rm in}(j',i')\rangle + \mathcal{C}(j,j';i,i'). \quad (4.1)$$

We see that, since all elements $\mathcal{C}(j,j')$ are small provided $\Delta \geq l_c$, the teleportation preserves the spatio-temporal pixel correlation. The same holds also for the higher-order correlation functions since the added noise is Gaussian and independent from the input.

This conclusion is based on the added noise power. Some other criteria for the quantum teleportation were suggested in the literature, see e.g. [27].

The quality of reconstruction of the quantum state $|\Psi_{\rm in}\rangle$ of the input field in the teleportation process is usually quantified via the fidelity parameter F. For simplicity we consider here the fidelity of teleportation of a pure quantum state, which is defined as

$$F = |\ \langle\Psi_{\rm in}|\Psi_{\rm out}\rangle\ |^2\ . \tag{4.2}$$

This definition works well for teleportation of a single degree of freedom of the quantized field. But in our case of quantum teleportation of a multimode light field, distributed in space and time, the definition (4.2) meets some obvious difficulties that stem from the multimode nature of the field. Let us for instance assume that the input state to be teleported has no correlation in space and time (as e.g. for a coherent image), and that our teleportation protocol does not add any correlations between spatial and/or temporal modes (as it happens for a large enough detection time window and pixel side). In this case the global fidelity of the teleportation protocol factorizes in the product of the single-mode fidelities. Even if each mode is teleported with almost perfect fidelity, close, but slightly less than unity, the global fidelity in the limit of a large number of modes will be close to zero, and will always reduce to zero for an infinite number of modes. For this reason, in the case of quantum teleportation of a multimode field it is important to identify the relevant set of degrees of freedom and to introduce the notion of the reduced fidelity for this set of degrees of freedom, and of the average fidelity per mode.

An alternative definition of fidelity can be given in terms of the superposition of the Wigner functions describing the state in the input and in the output (see e.g. [3]).

We can introduce the Wigner function of the output field as a quasi-probability distribution in the multidimensional space of the discrete set of real variables x_{ji}, y_{ji}, $(j = 1, N;\ i = 1, K)$, that correspond in the Wigner representation to orthogonal field quadratures measured over jth pixel and ith time interval. It is defined as the Fourier transform in the $N \times K$ dimensional space of a characteristic function:

$$W^{\rm out}\left(\{x_{ji}, y_{ji}\}\right) = \int \frac{{\rm d}^{N\times K}\mu}{(2\pi)^{N\times K}} \int \frac{{\rm d}^{N\times K}\nu}{(2\pi)^{N\times K}} \times \exp\left\{-{\rm i}\sum_{i,j}[\mu_{ji}x_{ji} + \nu_{ji}y_{ji}]\right\} \chi_{\rm out}\left(\{\mu_{ji}, \nu_{ji}\}\right), \tag{4.3}$$

where the symmetrically ordered characteristic function is defined by:

$$\chi_{\rm out}\left(\{\mu_{ji}, \nu_{ji}\}\right) = \left\langle \exp\left\{{\rm i}\sum_{i,j}\left[\mu_{ji}X^{\varphi}_{\rm out}(j,i) + \nu_{ji}Y^{\varphi}_{\rm out}(j,i)\right]\right\}\right\rangle, \tag{4.4}$$

with analogous definitions for the input. By using the relations (3.24) and (3.25) linking the quadrature operators of the teleported field to those of the input, and the fact that the excess noise operators are independent from the input ones, we obtain

$$\begin{aligned}\chi_{\rm out}\left(\{\mu_{ji}, \nu_{ji}\}\right) = &\left\langle \exp\left\{{\rm i}\sum_{i,j}\left[\mu_{ji}X^{\varphi}_{\rm in}(j,i) + \nu_{ji}Y^{\varphi}_{\rm in}(j,i)\right]\right\}\right\rangle \\ &\times \left\langle \exp\left\{{\rm i}\sum_{i,j}\left[\mu_{ji}\mathcal{X}(j,i) + \nu_{ji}\mathcal{Y}(j,i)\right]\right\}\right\rangle \\ &= \chi_{\rm in}\left(\{\mu_{ji}, \nu_{ji}\}\right)\chi_{\rm noise}\left(\{\mu_{ji}, \nu_{ji}\}\right),\end{aligned} \tag{4.5}$$

where $\chi_{\rm noise}\left(\{\mu_{ji}, \nu_{ji}\}\right)$ is the characteristic function of the Gaussian distribution of the excess noise, given by (3.29). Hence the Wigner function of the teleported field is given by a convolution of the Wigner function of the input field with a multivariate Gaussian distribution, with zero mean and covariance matrix given by (3.31). An analogous relation holds for other quasi-probability distributions in phase-space, that correspond to different ordering of operators (e.g. for antisymmetrical ordering, the Husimi Q-function); however, since F, $F^{\dagger}$ are commuting operator, ordering is irrelevant for $\chi_{\rm noise}\left(\{\mu_{ji}, \nu_{ji}\}\right)$.

The fidelity parameter that quantifies the quality of the teleportation process is thus given by

$$\begin{aligned}F &= (4\pi)^{N\times K}\int {\rm d}^{N\times K}x \int {\rm d}^{N\times K}y \\ &\quad\times W^{\rm out}\left(\{x_{ji}, y_{ji}\}\right) W^{\rm in}\left(\{x_{ji}, y_{ji}\}\right) \\ &= \frac{1}{\pi^{N\times K}}\int {\rm d}^{N\times K}\mu \int {\rm d}^{N\times K}\nu \\ &\quad\times \chi_{\rm out}\left(\{\mu_{ji}, \nu_{ji}\}\right)\chi_{\rm in}\left(\{-\mu_{ji}, -\nu_{ji}\}\right) \\ &= \frac{1}{\pi^{N\times K}}\int {\rm d}^{N\times K}\mu \int {\rm d}^{N\times K}\nu \\ &\quad\times \left|\chi_{\rm in}\left(\{\mu_{ji}, \nu_{ji}\}\right)\right|^2 \chi_{\rm noise}\left(\{\mu_{ji}, \nu_{ji}\}\right),\end{aligned} \tag{4.6}$$

where the last line has been obtained by using the relation (4.5) relating input and output characteristic functions.

Notice that in the limit of no excess noise $\mathcal{C}(j, j'; i'i') = 0$, $\chi_{\rm noise} = 1$, and we have

$$\begin{aligned}F &= \frac{1}{\pi^{N\times K}}\int {\rm d}^{N\times K}\mu \int {\rm d}^{N\times K}\nu\, \left|\chi_{\rm in}\left(\{\mu_{ji}, \nu_{ji}\}\right)\right|^2 \\ &= {\rm Tr}\left\{\hat{\rho}^2_{\rm in}\right\} = 1\end{aligned} \tag{4.7}$$

for a pure input state ($\hat{\rho}_{\rm in} = |\Psi_{\rm in}\rangle\langle\Psi_{\rm in}|$ is the input field density matrix). In general, however, excess noise will be always present to some extent and $F < 1$. We can explicitly calculate the fidelity for Gaussian input states (e.g. squeezed states, coherent states, EPR beams),

for which

$$\chi_{\rm in}\left(\{\mu_{ji},\nu_{ji}\}\right)=\exp\left\{-\frac{1}{2}\sum_{j,j';i,i'}\left[V^X(j,j'\,;\,i,i')\mu_{ji}\mu_{j'i'}+V^Y(j,j'\,;\,i,i')\nu_{ji}\nu_{j'i'}\right]\right\},\quad(4.8)$$

where we have assumed without loss of generality that

$$\langle X_{\rm in}(j,i)\rangle=\langle Y_{\rm in}(j,i)\rangle=0\,,\qquad(4.9)$$

since the teleportation process preserves the mean values, and

$$\begin{aligned}\langle X_{\rm in}(j,i)\,X_{\rm in}((j',i')=V^X(j,j'\,;\,i,i')\rangle\,,\\ \langle Y_{\rm in}(j,i)\,Y_{\rm in}((j',i')=V^Y(j,j'\,;\,i,i')\rangle\,,\end{aligned}\qquad(4.10)$$

are the input covariance matrices. By using equation (4.6) and standard properties of Gaussian integrals we easily obtain

$$F=\frac{1}{\det\left[V^X(j,j'\,;\,i,i')+\frac{1}{2}\mathcal{C}(j,j';i,i')\right]^{\frac{1}{2}}}\times\frac{1}{\det\left[V^Y(j,j'\,;\,i,i')+\frac{1}{2}\mathcal{C}(j,j';i,i')\right]^{\frac{1}{2}}}.\qquad(4.11)$$

In particular for an input multimode coherent state $V^X(j,j'\,;\,i,i')=V^Y(j,j'\,;\,i,i')=\delta_{j,j'}\delta_{i,i'}$, and

$$F=\frac{1}{\det\left[\delta_{j,j'}\delta_{i,i'}+\frac{1}{2}\mathcal{C}(j,j';i,i')\right]}.\qquad(4.12)$$

These results have to be compared with the results of a classical teleportation protocol, that is, in the absence of EPR correlations, where $\mathcal{C}_{cl}(j,j';i,i')=2\delta_{j,j'}\delta_{i,i'}$. For a coherent input, in the classical case we have

$$F_{cl}=\frac{1}{2^{N\times K}}.\qquad(4.13)$$

From the above formulas it should be clear the claim that we made at the beginning of this section, that is, the global fidelity may approach rapidly zero for large number of degrees of freedom, and hence loose any quantitative meaning. A good strategy is to identify the relevant degrees of freedom of the system. If for instance the state to be teleported is the quantum state of coherent image, restricted to an array of N_A pixels, no one will be probably interested to the quality of teleportation of the vacuum state of the region of space outside the image.

Since we assumed a plane-wave pump, our model is translationally space and time invariant, and the number of available pixels and time intervals is in principle infinite. This kind of model describes well a realistic system, provided that the pump spot size is much larger than the amplifier coherence area and that the pump pulse duration is much longer than the amplifier coherence time [16]. Obviously, one has also to require that the beam whose state is to be teleported is well confined inside the region where significant gain is available, both in space and time.

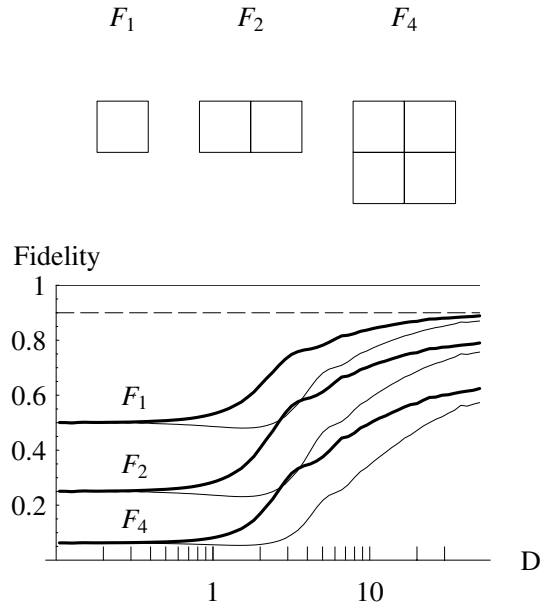

Fig. 5. Reduced fidelity of quantum holographic teleportation for patterns of 1, 2, and 4 pixels, shown on the top of the figure (plots F_1, F_2, and F_4 respectively), as a function of $D=\Delta/l_d$. The squeezing parameter is $\exp[r(0,0)]=3$.

Let us assume to divide our system in two subsystems, say A and B, where subsystem A corresponds to a subset $\{j,i\}_A$ of pixels and of time intervals of interest for given measurement, and subsystem B is made of the remaining $\{j,i\}_B$ pixels and time intervals. By tracing out over the degrees of freedom of subsystem B, the characteristic function describing the statistical properties of the subsystem A alone is obtained as:

$$\chi^A_{\rm in}\left(\{\mu_{ji},\nu_{ji}\}_A\right)=\mathrm{Tr}_A\left\{\left[\mathrm{Tr}_B\hat{\rho}_{\rm in}\right]\exp\left\{\mathrm{i}\sum_{\{j,i\}_A}\left[\mu_{ji}X^{\varphi}_{\rm in}(j,i)+\nu_{ji}Y^{\varphi}_{\rm in}(j,i)\right]\right\}\right\}=\chi_{\rm in}\left(\{\mu_{ji},\nu_{ji}\}_A\,\{\mu_{ji}=0,\nu_{ji}=0\}_B\right),\qquad(4.14)$$

and similarly for the output. By repeating all the passages (4.5) and (4.6) that allowed us to calculate the fidelity, but for the reduced characteristic function, we easily conclude that the formulas (4.11) and (4.12) hold true for the fidelity of the reduced set of degrees of freedom, provided that the covariance matrices in those formulas are the covariance matrices of the second-order moments of operators on the pixels and time intervals of subsystem A.

In Figure 5 we show the reduced fidelity dependence on the pixel size and on the number of pixels for some simple patterns of pixels, in the case of a coherent image in the input. The observation, as in Figures 4a and 4b is assumed to be performed within the same time window, so that the dimension of the covariance matrix in our case is given by the number of pixels in the pattern. This is very

reasonable for a traveling-wave OPA, since in a realistic configuration in order to obtain large gain a pulsed operation is required. Therefore, the detection time window will be probably longer or of the same order as duration of the pump pulse. Notice that the same is not necessarily true for a cavity configuration, because the CW operation in this case permits to resolve temporal degrees of freedom.

The shape of the patterns for 1, 2, and 4 pixels is shown on the top of Figure 5. We plot our numerical calculations of F_A given by equation (4.11) for the degree of squeezing $\exp[r(0,0)] = 3$, as a function of the ratio of the pixel side to the diffraction length $D = \Delta/l_d$. For these patterns only the diagonal covariance matrix elements $\mathcal{C}(j,j)$, and those describing nearest neighbor correlations in a row, in a column and in a diagonal are of importance. The wide and narrow solid lines correspond to the observation with (wide lines) and without (narrow lines) diffraction phase shift compensation with the use of a lens arrangement. For small pixel size, $D \ll 1$, all curves attain the classical limit $F_N \to 0.5^N$. For large pixel size, $D \gg 1$, the curves tend to the limit, imposed by the degree of squeezing: $F_N \to (1 + \exp[-2r(0,0)])^{-N} = 0.9^N$. As seen from Figure 5, the fidelity of teleportation decreases with the number of pixels. This qualitatively means that the multi-pixel observables, dependent on the correlations between pixels, are more sensitive to the absence of entanglement in the quantum channel than the observables for a single pixel.

The effect of optimization of the spatial scales in our teleportation protocol with the use of a lens arrangement is significant for a pixel width $\Delta \approx l_c$. As shows Figure 5, the optimization allows us to achieve the same value of fidelity for the pixel size, smaller by factor (2...3) than in absence of such optimization.

As it is clear from inspection of the curves in Figure 5, the fidelity for N degrees of freedom scales with the Nth power. A significant quantity to plot is hence the average fidelity per pixel, that is

$$F_{\rm av} = (F_N)^{\frac{1}{N}} . \tag{4.15}$$

Consider a single temporal degree of freedom $K = 1$. For a large $N = M \times M$ array of square pixels, the covariance matrix becomes translationally invariant, and it can be diagonalized by means of a discrete Fourier transformation. Let us consider periodic boundary conditions, and introduce

$$\lambda(\vec{q}_{\vec{n}}) = \sum_{\vec{j}} \mathcal{C}(\vec{j},0) e^{-i\vec{q}_{\vec{n}}\cdot\vec{\rho}_{\vec{j}}} . \tag{4.16}$$

Here $\vec{j} = (j_x, j_y)$, with $j_{x,y}$ an integer, is a 2D label of the pixel position. The 2D wave vector of the eigenwave is given by $\vec{q}_{\vec{n}} = (2\pi/M\Delta)\vec{n}$, where $\vec{n} = (n_x, n_y)$, with $n_{x,y}$ an integer, and $|n_{x,y}| \le (M-1)/2$ (we take M odd for simplicity). In terms of continuous Fourier transform equation (4.16) reads,

$$\lambda(\vec{q}) = \int d\vec{\rho} \left\{ \sum_{\vec{j}} \delta(\vec{\rho} - \vec{\rho}_{\vec{j}}) \right\} \mathcal{C}(\vec{\rho},0) e^{-i\vec{q}\cdot\vec{\rho}}, \tag{4.17}$$

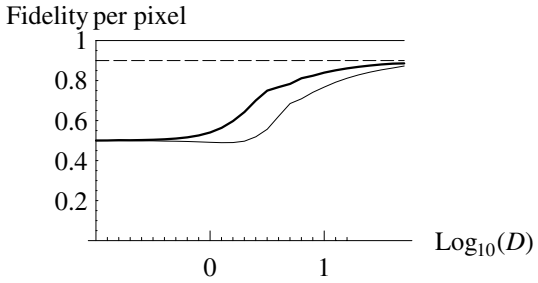

Fig. 6. Average fidelity per pixel for the quantum holographic teleportation of a large number of pixels in a coherent state as a function of $D = \Delta/l_d$. The squeezing parameter is $\exp[r(0,0)] = 3$.

and is related to the convolution of the Fourier transforms of the factors in the integrand. Here we use the relation

$$\int d\vec{\rho} \left\{ \sum_{\vec{j}} \delta(\vec{\rho} - \vec{\rho}_{\vec{j}}) \right\} e^{-i\vec{q}\cdot\vec{\rho}} = \left(\frac{2\pi}{\Delta}\right)^2 \sum_{\vec{m}} \delta\left(\vec{q} - \frac{2\pi}{\Delta}\vec{m}\right), \tag{4.18}$$

where $\vec{m} = (m_x, m_y)$, with $m_{x,y}$ integer. The Fourier transform of $C(\vec{\rho},0)$ is easily evaluated from (3.31). After some calculation we obtain

$$\lambda(\vec{q}) = 2 \sum_{\vec{m}} \mathrm{sinc}^2\left(\frac{q_x\Delta}{2} - \pi m_x\right) \times \mathrm{sinc}^2\left(\frac{q_y\Delta}{2} - \pi m_y\right) \tilde{G}\left(\vec{q} - \frac{2\pi}{\Delta}\vec{m}\right). \tag{4.19}$$

In the limit $M \to \infty$, the average fidelity per pixel is found in the form

$$F_{\rm av} = \prod_{\vec{n}} \left(1 + \frac{1}{2}\lambda(\vec{q}_{\vec{n}})\right)^{-1/N} = \exp\left\{ -\left(\frac{\Delta}{2\pi}\right)^2 \int\limits_{|q_{x,y}| \le \pi/\Delta} d\vec{q} \ln\left(1 + \frac{1}{2}\lambda(\vec{q})\right) \right\}. \tag{4.20}$$

Figure 6 shows the behavior of the average fidelity per pixel for quantum teleportation of a large array of pixels in a coherent state.

5 Conclusions

In this paper we have provided a detailed analysis of the quantum fluctuations in the holographic teleportation technique for optical images proposed in [11]. A fundamental result of this treatment is the quantitative evaluation of the fidelity of the quantum state transfer. This was obtained, first all, by deriving the statistics of the excess noise from a a characteristic functional, both in a continuous and in a coarse-grained description of the spatio-temporal degrees of freedom of the optical field.

As a second step, we calculated the Wigner function of the teleported field from that of the input field, which in turns enabled us to derive an explicit formula for the fidelity of the multimode teleportation process. Such a fidelity depends on the number and choice of the image elements that one teleports in parallel.

On the one side, we find that an optimal fidelity can be reached only when the transverse size of the image pixels to be teleported is not smaller than the coherence length of the EPR entangled beams used in the protocol. This limit on the spatial resolution of the scheme is imposed by the limited spatial bandwidth of emission of the parametric amplification process used to generate the EPR beams. The limitations on the spatial resolution of the device were already analysed in [11], where criteria for minimizing the excess noise were formulated. Here we derive the same limits in the context of a quantitative evaluation of the fidelity.

On the other side, we show that the fidelity of the multimode teleportation protocol is more sensitive to the lack of entanglement in the quantum channel, and to any other imperfection of the scheme, than that of the single-mode teleportation. Actually, the fidelity of the quantum state transfer of N pixels scales as the Nth power. It is therefore important to define a reduced fidelity of teleportation, related to the essential degrees of freedom to be teleported that can be defined, for example, by restricting the level of resolution of the input image in case of image teleportation. By properly matching the spatial bandwidth of the image to be teleported to that of the EPR beams, and by properly optimizing the scheme, we show that such a reduced fidelity can approach values very close to unity in our scheme.

The authors thank Denis Vasil'ev for assistance in the evaluation of fidelity in Section 4 of the paper. This work was supported by the Network QUANTIM (IST-2000-26019) of the European Union, by the INTAS under Project 2001-2097, and by the Russian Foundation for Basic Research under Project 03-02-16035.

Appendix A: Homodyne detection with spatial resolution

In this appendix we shall discuss the validity of equation (3.2) for the photocurrent density operators in the balanced homodyne detection scheme with spatial resolution. For definiteness we shall consider the homodyne detection of the X quadrature component. The results for the conjugate component are obtained in the similar way. In Figure 7 we present in detail the schematic of the "point-by-point" balanced homodyne detection with a photodetector D_x. To achieve the spatial resolution, the pixels of the CCD matrices are assumed to be much smaller than the coherence area S_c of the EPR beams. We shall discuss the properties of the quantum operator for the surface density of the photocurrent and show, that the definition (3.2) of this observable is in agreement with

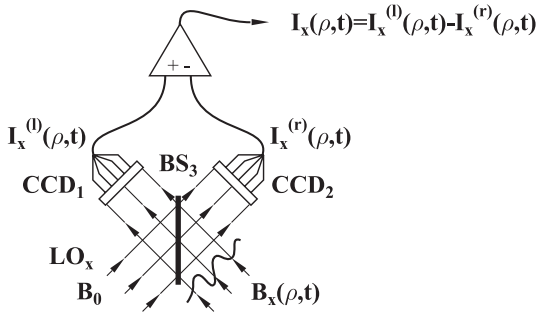

Fig. 7. Schematic of balanced homodyne detection with spatial resolution.

the standard description of photodetection with resolution in space and time, based on the Glauber field correlation functions [28]. The output signal of the balanced homodyne detector D_x is given by

$$I_x(\vec{\rho},t) = I_x^{(l)}(\vec{\rho},t) - I_x^{(r)}(\vec{\rho},t), \tag{A.1}$$

where $I_x^{(l)}(\vec{\rho},t)$ and $I_x^{(r)}(\vec{\rho},t)$ are the surface photocurrent densities, measured by the left and right CCD matrices. The local oscillator plane wave LO_x with complex amplitude $B_x^{(H)}$ is classical and strong, $|B_x^{(H)}| \gg |B_x(\vec{\rho},t)|$, where $B_x(\vec{\rho},t)$ is the input field of the detector. In this limit the quantum operator for the difference photocurrent surface density is introduced in analogy to the earlier investigated spatially single-mode case, see [23] and in more general context [24]. The classical field strength is replaced by the quantum field operator $B_x(\vec{\rho},t)$ in the difference surface power of beatings between the object and the local oscillator waves:

$$I_x(\vec{\rho},t) = {B_x^{(H)}}^* B_x(\vec{\rho},t) + \mathrm{h.c.} \tag{A.2}$$

The quantum efficiency of the CCD matrices for simplicity is assumed to be equal to unity and the additional quantum noise due to the light losses in detectors is neglected. The beam splitter BS_3 is described by the matrix similar to (2.16).

Let us show, that the operator (A.2) is in agreement with the Glauber photodetection theory [28] and, in particular, describes correctly the shot noise of photodetection in space and time. In standard photodetection theory the second-order correlation function of the photocurrent density is related to the fourth-order correlation function of the field amplitudes. In our case of differenced photodetection this relation reads,

$$\begin{aligned}\left\langle \frac{1}{2}\left\{I_x(\vec{\rho},t), I_x(\vec{\rho}',t')\right\}_+ \right\rangle &= \langle \Phi_x^{(l)}(\vec{\rho},t) + \Phi_x^{(r)}(\vec{\rho},t)\rangle \delta(\vec{\rho}-\vec{\rho}')\delta(t-t') \\ &+ \left\langle T_N \left\{ \left(\Phi_x^{(l)}(\vec{\rho},t) - \Phi_x^{(r)}(\vec{\rho},t)\right) \right.\right. \\ &\left.\left. \times \left(\Phi_x^{(l)}(\vec{\rho}',t') - \Phi_x^{(r)}(\vec{\rho}',t')\right) \right\} \right\rangle. \end{aligned} \tag{A.3}$$

Here the quantities

$$\Phi_x^{(l)}(\vec{\rho},t)=\frac{1}{2}\Big(B_x^{(H)}+B_x(\vec{\rho},t)\Big)^{\dagger}\Big(B_x^{(H)}+B_x(\vec{\rho},t)\Big),$$
$$\Phi_x^{(r)}(\vec{\rho},t)=\frac{1}{2}\Big(-B_x^{(H)}+B_x(\vec{\rho},t)\Big)^{\dagger}\Big(-B_x^{(H)}+B_x(\vec{\rho},t)\Big), \tag{A.4}$$

are the surface densities of the photon flux on the left and right CCD matrices, and $\{...,...\}_+$ stands for the anticommutator. The T_N ordering of the field operators in (A.3) means: (i) the normal ordering, and (ii) the time ordering of the positive-frequency (annihilation) operators, such that the time argument grows up from right to left, and the inverse time ordering of the negative-frequency (creation) field operators.

In the limit of a strong local oscillator we can assume in (A.3) the following approximation:

$$\Phi_x^{(l)}(\vec{\rho},t)-\Phi_x^{(r)}(\vec{\rho},t)\approx {B_x^{(H)}}^{*}B_x(\vec{\rho},t)+\text{h.c.} \tag{A.5}$$

Consider now the same second-order symmetrized correlation function of the output photocurrents [see the left side of (A.3)], directly substituting into it the introduced above surface photocurrent density operator (A.2). Bringing the field operators to the T_N order with the use of the commutation relation similar to (2.1), we arrive at

$$\left\langle\frac{1}{2}\left\{I_x(\vec{\rho},t),I_x(\vec{\rho}\,',t')\right\}_+\right\rangle=|{B_x^{(H)}}^{*}|^2\delta(\vec{\rho}-\vec{\rho}\,')\delta(t-t')$$
$$+\left\langle T_N\left\{\left({B_x^{(H)}}^{*}B_x(\vec{\rho},t)+\text{h.c.}\right)\right.\right.$$
$$\left.\left.\times\left({B_x^{(H)}}^{*}B_x(\vec{\rho}\,',t')+\text{h.c.}\right)\right\}\right\rangle. \tag{A.6}$$

This expression agrees with the Glauber correlation function (A.3), approximated with the use of (A.5). The delta-like contribution describes the shot noise of photodetection in space and time. In Section 3 we apply the difference photocurrent surface density operator (A.2) to analysis of our teleportation scheme.

References

1. C.H. Bennett, G. Brassard, C. Crepeau, R. Jozsa, A. Peres, W.K. Wooters, Phys. Rev. Lett. **70**, 1895 (1993)
2. L. Vaidman, Phys. Rev. A **49**, 1473 (1994)
3. S.L. Braunstein, H.J. Kimble, Phys. Rev. Lett. **80**, 869 (1998)
4. D. Bouwmeester et al., Nature **390**, 575 (1997); D. Boschi et al., Phys. Rev. Lett. **80**, 1121 (1998)
5. A. Furusawa, J.L. Sorensen, S.L. Braunstein, C.A. Fuchs, H.J. Kimble, E.S. Polzik, Science **282**, 706 (1998)
6. W.P. Bowen, N. Treps, B.C. Buchler, R. Schnabel, T.C. Ralph, H.-A. Bachor, T. Symul, P.K. Lam, Phys. Rev. A **67**, 032302 (2003)
7. S.L. Braunstein, Phys. Rev. Lett. **80**, 4084 (1998); S.L. Braunstein, Nature **394**, 47 (1998); S. Lloyd, J.-J.E. Slotine, Phys. Rev. Lett. **80**, 4088 (1998)
8. S.L. Braunstein, H.J. Kimble, Phys. Rev. A **61**, 042302 (2000)
9. T.S. Ralph, Phys. Rev. A **61**, 010303(R) (1999)
10. P. Van Loock, S.L. Braunstein, H.J. Kimble, e-print `arXiv:quant-ph/9902030`
11. I.V. Sokolov, M.I. Kolobov, A. Gatti, L.A. Lugiato, Opt. Commun. **193**, 175 (2001)
12. M.I. Kolobov, I.V. Sokolov, JETP **69**, 1097 (1989); M.I. Kolobov, I.V. Sokolov, Phys. Lett. A **140**, 101 (1989)
13. M.I. Kolobov, Rev. Mod. Phys. **71**, 1539 (1999)
14. E. Brambilla, A. Gatti, P. Navez, L.A. Lugiato, Phys. Rev. A **65**, 013813 (2002); e-print `arXiv:quant-ph/0010108`
15. M.I. Kolobov, Phys. Rev. A **44**, 1986 (1991)
16. E. Brambilla, A. Gatti, L.A. Lugiato, Phys. Rev. A **69**, 023802 (2004)
17. See e.g. Chonghoon Kim, Prem Kumar, Phys. Rev. Lett. **73**, 1605 (1994) for a review of the problem
18. L.A. Lugiato, Ph. Grangier, J. Opt. Soc. Am. B **14**, 225 (1997)
19. K.I. Petsas, A. Gatti, L.A. Lugiato, C. Fabre, Eur. Phys. J. D **22**, 501 (2003)
20. A. Gatti, S. Gigan, A. Maitre, C. Fabre, *Effect of finite length of nonlinear medium on the multimode squeezing properties of a confocal OPO*, in preparation
21. I.V. Sokolov, M.I. Kolobov, L.A. Lugiato, Phys. Rev. A **60**, 2420 (1999)
22. A.V. Belinskii, N.N. Rosanov, Opt. Spektrosk. **73**, 153 (1992) [Opt. Spectrosc. **73**, 89 (1992)]
23. B. Yurke, Phys. Rev. A **32**, 311 (1985)
24. S.Z. Ou, H.J. Kimble, Phys. Rev. A **52**, 3126 (1995)
25. M.I. Kolobov, I.V. Sokolov, Europhys. Lett. **15**, 271 (1991)
26. A. Gatti, L.A. Lugiato, Phys. Rev. A **52**, 1675 (1995)
27. T.C. Ralph, P.K. Lam, Phys. Rev. Lett. **81**, 5668 (1998)
28. R.J. Glauber, Phys. Rev. **130**, 2529 (1963); R.J. Glauber, in *Quantum Optics and Electronics*, Les Houches Summer School of Theoretical Physics, University of Grenoble, edited by C. DeWitt, A. Blandin, C. Cohen-Tannoudji (Gordon and Breach, New York, 1965), p. 53